Lab on a Chip

Design of a 2D no-flow chamber to monitor hematopoietic stem cells

Journal:	*Lab on a Chip*
Manuscript ID:	LC-ART-07-2014-000807.R2
Article Type:	Paper
Date Submitted by the Author:	11-Sep-2014
Complete List of Authors:	Cambier, Théo; CEA, iRTSV Honegger, Thibault; CNRS, LTM Vanneaux, Valerie; APHP, IUH Berthier, Jean; CEA, LETI PEYRADE, David; LTM-CNRS, Blanchoin, Laurent; CEA, iRTSV Larghero, Jerome; APHP, IUH Thery, Manuel; CEA, iRTSV

Design of a 2D no-flow chamber to monitor hematopoietic stem cells

Théo Cambier[1], Thibault Honegger[2], Valérie Vanneaux[3], Jean Berthier[4], David Peyrade[2], Laurent Blanchoin[1], Jerome Larghero[3] and Manuel Théry[1,3]

1 – Laboratoire de Physiologie Cellulaire et Végétale, Institut de Recherche en Technologie et Science pour le Vivant, UMR5168, CEA, INRA, CNRS, Université Grenoble-Alpes, Grenoble, France
2 - Laboratoire des Technologies de la Microélectronique, CNRS, CEA, Université Grenoble-Alpes, Grenoble, France.
3 - Unité de Thérapie Cellulaire et Centre d'Investigation Clinique en Biothérapies, Hôpital Saint Louis, Institut Universitaire d'Hematologie, UMRS1160, INSERM, AP-HP, Université Paris Diderot, Paris, France.
4 - Laboratoire d'Electronique et de Technologie de l'Information, CEA, Université Grenoble-Alpes, Grenoble, France.

Abstract

Hematopoietic stem cells (HSC) are the most commonly used cell type in cell-based therapy. However, the investigation of their behavior in vitro has been limited by the difficulty to monitor these non-adherent cells in classical culture conditions. Indeed, fluid flow moves cells away from the video-recording position and prevents single cell tracking over long time periods. Here we describe a large array of 2D no-flow chambers allowing the monitoring of single HSC during several days. Chamber design has been optimized to facilitate manufacturing and routine use. The chip contains a single inlet and 800 chambers. Chamber medium can be renewed by diffusion in few minutes. This allowed us to stain live human HSCs with fluorescent primary antibodies in order to reveal their stage in the hematopoiesis differentiation pathway. Thereby we could correlate human HSC growth rate, polarization and migration to their differentiation stage.

Introduction

Blood, milk, lymph, urine, sweat and mucus are some of the body fluids that run across our organs and tissues. Fluid flow is intimately coupled to cell function and organ physiology. Cells produce, sense and response to fluid flow in various ways. Fluid flow generates a shear stress on adherent cells, such as epithelial or endothelial cells, which tend to align their shape and polarity with respect to the flow [1]. The shear stress also regulate cell size [2], cell proliferation and differentiation [3] and thereby tissue patterning [4] and morphogenesis [5]. By contrast, most cells of the lymphoid and myeloid lineages are less adhesive and thus much less resistant to high fluid-flow induced shear stress. They are transported along the blood flow and home in flow-protected regions in adjacent tissues. The shear stress modulates leukocytes adhesion, architecture and migration properties [6]. This sensitivity to fluid flow is a matter of concern in classical cell culture conditions where temperature-induced convection permanently displaces cells. These movements prevent long term monitoring of their behavior in video-microscopy. In addition, they are also likely to have consequences on hematopoietic stem cells (HSCs) differentiation since shear stress, and mechanical forces in general, are major regulator of stem cells fate [7–9] . The analysis and control of HSC fate is of paramount importance since HSC are currently the most commonly used cell type of stem cell based therapy [10,11]. HSC have been used clinically since 1959 and it is now established as a standard therapeutic modality for a variety of malignant and non-malignant diseases [12]. Our incapacity to protect HSC from fluid flow and monitor single cell behavior as they are submitted to biochemical signals is a serious matter of concern. While numerous microfluidic devices have been designed to control the flow speed and shear stress applied on adherent cells [13], much less attempts have been made to completely stop the flow in order to monitor and analyze HSCs in their unbiased state.

Multi-layered chips with fluidic valves have been used to start/stop the flow and isolate reaction chambers [14]. HSCs have also been protected from fluid flow in the bottom of deep microwells. Multi-layered chips were used to start/stop the flow above the wells, load HSCs and test the influence of several combinations of soluble factors in parallel [15]. Multi-layer chips have also been used to supply cells with soluble factors through a porous membrane protecting cells from convection flow [16]. The same concept was applied to single layer chips in which the supply channels were connected to a reaction chamber via several thin channels in which the flow was very low [17]. Simpler devices, made of a single layer of channels of equal height, were also tested. As an alternative to thin channels, alignments of pillars were used to separate the supply channels from the reaction channel and limit the flow in between them [18,19]. In some other devices, the flow was prevented by using dead-end channels as reaction chambers [20,21]. All these devices have pros and cons. To be usable in a routine basis in biology, the device has to be easy and fast to manufacture. It also has to be robust and should allow the visualization of numerous chambers in parallel. Here we describe a 2D chip, with a single inlet and 800 no-flow chambers per square-centimeter.

Materials and Methods

No-flow chamber manufacturing

The thick positive resist AZ9260 (AZ Electronic materials) was spin-coated on a 4-inch silicon wafer at 750 rpm for 60 s to obtain a 20 microns thick layer. It was pre-baked on a hot plate during 1 min at 60°C and then 4 min at 110°C. It was exposed to UV through a photomask (Toppan) baring the features of interest during 50s (35 mW/mm² at 405 nm and 16 mW/mm² at 365 nm) on a mask aligner (MJB4, SussMicroTec), developed in AZ400K 1:4 (AZ Electronic materials) for 60 s and washed with deionized water. The developed resist is finally dried with air-blow.

Poly-dimethyl siloxane (PDMS) (kit sylgard 184, Dow Corning) was mixed with the curing agent (10:1 ratio), degassed, poured onto the mold and cured for 1h at 100°C on a hot plate. The PDMS layer was then peeled off and stored away from the dust. The PDMS chip and a standard glass slide (76x26 mm borosilicate) were oxidized in an oxygen plasma cleaner for 10s at 100W (Femto, Diener Electronics) and placed into contact to ensure bonding and prevent fluidic leakage. Prior to bonding, the PDMS chip was punched with punch hole (Ted Pella) with outer diameter smaller than 1/16'.

The PDMS chip device was then connected to a pump setup via microfluidic capillaries (ID 100 um OD 1/16', Upchurch) by inserting the capillary in the punch hole. The PDMS elasticity prevented fluidic leakage by exerting pressure on the capillary. The other side of the capillary was connected to a half filled reservoir where controlled pressurized air would fill the capillary and the chip at a linear flow rate. Air pressure in the reservoir was control by a homemade pumping setup based on a motorized pump (Tecan XP3000) remotely controlled by a computer.

The chip were first filled with deionised water and then perfused with targeted medium. To allow changing from one medium to the other without inserting bubble, a 4 way valve (Upchurch) was inserted in-line so that the pressure from the pump was redirected to another reservoir containing the new media.

HSC isolation and culture

Human umbilical cord blood samples were collected from normal full-term deliveries after maternal informed consent according to approved institutional guidelines (Assistance Publique – Hôpitaux de Paris, Paris, France). CD34+ cells were isolated using the direct CD34 Progenitor Cell Isolation Kit (Miltenyi Biotec, Paris, France) and cryopreserved in SVF (Hyclone)/10% DMSO (B Braun). After thawing, cells were resuspended in the culture medium HPO1 (MacoPharma, France) supplemented with growth factors : 100 ng/µL SCF ; 10 ng/µL G-CSF ; 20 ng/µL TPO ; 100 ng/µL FLT3l (Peprotec) just before being injected in the microfluidic device at a density of 10^6 cells/mL.
CD34+ cells were stained with addition of PE-CD33, APC-CD34 and FITC-CD38 monoclonal antibodies (Becton Dickinson).

Image acquisition

Images were taken on a ECLIPSE Ti (Nikon) equipped with a confocal scanner unit (CSU-X1, Yokogawa), a 4-wavelength LED excitation device (CoolLED pE-2 collimator, Life sciences and analytical), and a CoolSnap HQ2 camera (Photometrics). Microscope was controlled using Metamorph software (Molecular Devices).

When it contained cells, the chip was maintained on the microscope on a heating stage and humidified chamber at 37 °C supplied with 5 % CO_2 for pH buffering (Live Cell Instrument).

Comsol simulations

Simulations of the fluid flow were performed by a finite element method using COMSOL Multiphysics (COMSOL). Each design was modeled in a 2D plane. A planar laminar flow was set up with the same input and output boundary flow conditions. A time-lapse diffusion model was monitored until full replacement of media in the chambers and asymmetric connecting micro-channels.

Results

No-flow chamber design

We refer here to a no-flow chamber as a confined space in which fluid flow is absent or comparable to thermal agitation (Figure 1A). Our aim was to design such a chamber in 2D with a minimum number of inlets/outlets to facilitate chamber manufacturing and use. We defined few key criteria for the design of the chamber. The no-flow chamber should contain one or several side channels for the supply of new solutes. Pressures should be balanced in order to restrict fluid flow to these side channels (Figure 1B). The size of the openings between the side channels and the chamber should protect the chamber from fluid entry. However, these openings should allow solutes diffusion from side channels to the chamber. Finally, the chamber size should allow fluid renewal by diffusion in few minutes (Figure 1C).

Compartmentalized microenvironments, protected from fluid flow by linear arrays of micropillars, have been designed to confine multicellular clusters of adherent cells [18]. The underlying concept is brilliant and proved to be quite efficient to confine these cell groups [19]. Numerical simulations revealed that in such a device a residual flow would persist and affect loosely adherent cells such as HSCs (Figure S1A). Physical barriers perpendicular to this residual flow in the chambers should reduce it (Figure S1B). Reducing the number of openings between side-channels and the main chamber should also reduce internal flow. Eventually, square chambers with two side openings, as shown in Figure 1A, appeared optimal (Figure S1D).

A single opening should even be more efficient than two openings to protect the chamber from fluid entry. Dead-end chambers with a single opening have been proved to be efficient to confine cells [20–22]. However they require the use of vacuum and porous material to remove the trapped air bubbles in the chambers and suck the cells inside.

Actually, trapped air bubbles constitute the most critical problem in no-flow devices, since they tend to form particularly in regions of interest where the flow is reduced. Intuitive symmetric designs in which no-flow chambers are flanked with two side-channels (Figure 1D), induce the trapping of air bubbles in most chambers. Indeed, the synchrony of fluid filling in the two symmetric side-channels immediately balances the pressure between the two openings and stops liquid flow in the central chamber, leading to air bubble trapping as illustrated in the sequence described in figure 1E. We designed asymmetric supply channels to circumvent this problem (Figure 1F). With asymmetric supply channels, fluid arrival close to the upper opening can be delayed so that the fluid fills in the chamber from the bottom opening (Figure 1G). The most straightforward way to ensure that the delay corresponds exactly to the time it takes to fill a chamber is to add one chamber, as a delay-line, to the upper supply channel (Figure 1F). In the time-sequence shown in figure 1H, fluorescently labeled proteins were used to show the filling of no-flow chambers with the asymmetric supply design (Movie S1). Almost no bubbles were trapped with these asymmetric side-channels. We also found that rounded chambers, rather than square chambers with right angles, improved chamber filling without trapping air bubbles (Figure S2).

The dimensions of the optimal chamber design are shown in figure S3A. Importantly our design offers the possibility to align chambers in series and to load many of those lines in parallel with a single inlet. We could thus design a $1cm^2$-chip with a single inlet distributing the fluid to 800 chambers (Figure 1I, 1J and figure S3B).

No-flow chamber test

The fluid flow in no-flow chambers was first estimated with numerical simulations. Fluid flow was present in the first three and the last three chambers of the line because of the asymmetric

supply but was almost absent from the 30 chambers in between (Figure S4A,B). In those chambers, the simulated flow in the supply channels barely entered the chambers (Figure S4C). This was further confirmed experimentally by looking at the motion of fluorescent beads (Figure 2A, movie S2). Long exposure during image acquisition revealed local bead displacements. Time-lapse acquisitions of such images revealed bead trajectories. Beads appeared almost immobile in the no-flow chambers whereas they were rapidly transported in the supply channels (Figure 2A). Measurements of bead displacement within chambers depending on their position along the supply channels confirmed that the 30 chambers at the center displayed no fluid flow even when the flow in the supply channel reached 1500µm/s (Figure 2B,C).

The possibility to renew the medium in no-flow chambers was tested by switching the inlet from green to red fluorophores (Figure 3A, movie S3). Since the new fluid could not flow through the chambers, the renewal was entirely supported by diffusion. We measured the green and the red fluorescent signals in the chamber (position A in figure 3B) and in the supply side-channels (position B). The chamber content appeared completely renewed 7 minutes after fluid switch. Larger chambers would have allow larger observation fields but would have make this renewal time much longer.

HSC loading and monitoring

The design of the chamber being optimized for fluid filling, flow blocking and medium renewal, we could introduce living cells in the no-flow chambers. As a first test, we used the Jurkat cell line, which are easy-to-use non-adherent human T lymphocytes. They could survive and proliferate in the no-flow chambers during several days. We then switched to human HSCs. Cells were collected from human umbilical cord blood, sorted based on the expression of CD34 [23] and immediately frozen in liquid nitrogen. CD34 is a cell surface glycoprotein from the family of sialomucins that is commonly used as a marker of stemness during hematopoiesis [24].

HSCs were thawed, resuspended in growth medium and loaded in no-flow chambers during initial chip filling. Cell density was adapted to obtain 1 to 10 cells per chamber (Figure 4A). Cell culture medium in side channels was renewed every 6 hours. Cell growth and movements were monitored in phase contrast microscopy over several days using multi-position time-lapse acquisitions (Figure 4B, movie S4). It appeared that HSC growth rates were highly variables: some cells divided up to six times in three days whereas other remained quiescent. To get further insights about the link between this variability and cell profiles diversity, we took advantage of the key feature of our new device to change cell culture medium without detaching non-adherent cells, and introduced fluorescently-labeled antibodies at the end of the acquisition (Figure 4C). These antibodies targeted various surface receptors known to reveal cell differentiation state. CD38 and CD34 were used are markers of non-differentiated cells [24] whereas CD33 was used as a mark of early engagement in the myeloid lineage [25].

Three days after cell collection and loading in the no-flow chambers most cells had started to express CD33, few cells were CD38 positive and only 60% were still expressing the stemness marker CD34. So the entire population appeared quite heterogeneous (Figure 4D). Several hypotheses could account for this diversity. It could be the consequence of asymmetric HSC divisions leading to daughter cells with distinct protein expression profiles. It could also be due to differences in the proliferation rates of distinct sub-populations. Clues could be obtained by tracking individual cells and reconstituting cell lineage trees (Figure 4E). Although some asymmetric divisions were observed (cell #5 in figure 4E for example), leading to daughter cells with distinct expression profile, they were quite rare and most of the clones displayed identical surface markers. This favored the differential grow rates hypothesis. To further test it, we counted the number of division the cells went through for all combinations of surface markers. Cells that were still expressing CD38 after three days did not divide or only once. Cells expressing CD34 went up to two rounds of divisions. By

contrast, cells expressing CD33 had divided two to four times (Figure 4F). These data accounted for the massive presence of CD33 cells after three days and suggested that population heterogeneity was mainly due to differences in cell proliferation capacities.

Cell monitoring revealed that most HSC acquired elongated and polarized leukocyte-like shapes soon after being loaded in the chip [26,27]. These cells developed dynamic membrane protrusions at their leading edge and displayed slow amoeboid-like migration throughout the no-flow chamber (Movie S4). By contrast, static cells remained round. Here also we took advantage of the possibility to associate cell monitoring with fluorescent immuno-staining to reveal the protein expression profiles of static and migrating cells. Three days after cell loading, the profiles of the static cells were heterogeneous: 60% were CD33+, 30% were CD33+/CD34+ (Figure 5A). Strikingly, 95% of migrating cells were CD33+/CD34+ (Figure 5A). So the co-expression of CD34 and CD33 did not seem to be specific to but characteristic of all moving cells. To further understand the relationship between CD33/CD34 co-expression and the acquisition of cell motility we looked at receptors localization at the cell surface. In static cells we could observe several patches of CD33, whereas in moving cells CD33 receptors were clustered at the cell rear in the uropod (Figure 5B). These observations were further quantified by the measurement of cell shape factor and surface marker distribution. Migrating cells appeared much more elongated than static cells (Figure 5C). Surface markers polarization was quantified by measuring the position of the center of mass of the fluorescence signal with respect to cell center. CD34 appeared evenly distributed in both static cells and migrating cells, whereas CD33 was strongly polarized toward the rear of migrating cells (Figure 5C). Backward polarization of CD33 in the uropod appeared as a specific signature of migrating CD34-positive HSCs.

Discussion

Here we described the design and use of a new no-flow chamber. Sophisticated microfluidic 3D chambers with several layers of channels and valves were used to screen multiple compounds on a chip [15]. The goal here was simply to protect the biological sample from fluid flow in a large array of chambers. The chambers shape and chip circuitry have been designed for routine use in biology. The aim was to minimize the manufacturing difficulties, and to make the chip robust and easy-to-use. The outcome of our work is a single-layer 2D chip, with a single inlet and 800 chambers per cm2 (the complete chip is visible in figure S3). The circuitry has been optimized to allow the fluid loading without formation of air bubbles. Since vacuum is not required to eliminate air bubbles the chip can be produced in plastic or glass as an alternative to PDMS. Finally, the chamber shape and size allow rapid medium exchange by diffusion. This last feature is particularly useful since it is almost impossible to change the fluid on top of flow sensitive biological samples in classical experimental conditions.

No-flow chambers are suited for biological systems that are sensitive to or could be damaged by fluid flow. For example, several biochemical assays are based on the detection of a specific protein or DNA strand in a sample thanks to its interaction with a surface-bound probe. These assays can be limited by the affinity between the probe and the ligand, particularly during the washing steps. Reducing fluid shear stress in no-flow chambers could improve the sensitivity of these assays. Another example relates to the cells types, such as endothelial or epithelial cells, which can be oriented in space or physiologically modified by fluid shear stress [13]. No flow chambers could be used to prevent such stress and get rid of this bias. Here we took advantage of the absence of flow to monitor HSCs, which are loosely adherent and therefore often displaced by fluid convection in classical cell culture conditions.

As HSC were used to validate the suitability of no-flow chambers for the monitoring of their behavior, we made two interesting observations that may have important implications in our understanding of stem cell physiology. First, the early rise in population heterogeneity seemed to involve mainly the differences in the proliferation rates of the various cell types. Second, HSC migration appeared coupled to cell shape polarization and rear clustering of CD33 receptors. These two observations fully validated the relevance of the no-flow chambers for the study of HSC physiology and opened new questions that remained to be investigated.

Human primary HSC were initially purified from umbilical cord blood samples by immuno-sorting based on the expression of CD34 according to the classical method that is commonly used in therapy protocols. The yield is known to be quite high and the initial proportion of CD34+ cells is around 90%. How this proportion decreased to 60% in three days is still not fully explained. CD34-/CD33+ cells proliferate quite fast and tend to predominate in the entire population. CD34+/CD33+ proliferate slightly slower and CD34+/CD33- divided rarely. This suggests that the expression of CD33 and the loss of expression of CD34 tend to be correlated to increased proliferation capacities. CD33+ cells are engaged in the myeloid lineage and somehow impair the regeneration capacities of bone marrow transplant. Further investigations are required to identify the mechanism underlying the early appearance of this marker and the loss of CD34 in order to prevent them and maintain the regeneration capacities of the transplant. The occurrence of asymmetric divisions in the very early stages of the cell culture is an attractive hypothesis that could account for the evolution we observed.

HSCs have been shown to display sometimes a polarized organization of cell surface receptor [28,29]. Several receptors, such as ICAMs, mucins, CD44 and integrins, were shown to cluster in the cholesterol-rich membrane of the uropod at the cell rear [28,30]. Our study showed that CD33 should be added to this list. More importantly, the long-term HSCs monitoring that was enabled by the absence of flow in the chambers revealed the tight coupling between this polarization and cell migration. This suggests that the early mechanisms involved in the initiation of cell migration are probably coupled to receptor clustering and cell polarization. Further studies are required to investigate the original symmetry break in HSCs. The association with cell migration suggests that the interplay between cell adhesion and contractility could be a key element in this event [31]. No-flow chambers offer the best-suited experimental conditions to study these basic and fundamental questions and improve our understanding of HSC biology.

Acknowledgements

MT and JL acknowledge supports of the European Research Council (Starting Grant ERC-310472) and the Agence National pour la Recherche (ANR-05PRIB01103, ANR-10-IBHU-0002). TC received a PhD fellowship from the president of Grenoble university.

References

1. M. a Ostrowski, N. F. Huang, T. W. Walker, T. Verwijlen, C. Poplawski, A. S. Khoo, J. P. Cooke, G. G. Fuller, and A. R. Dunn, *Biophys. J.*, 2014, **106**, 366–74.

2. C. Boehlke, F. Kotsis, V. Patel, S. Braeg, H. Voelker, S. Bredt, T. Beyer, H. Janusch, C. Hamann, M. Gödel, K. Müller, M. Herbst, M. Hornung, M. Doerken, M. Köttgen, R. Nitschke, P. Igarashi, G. Walz, and E. W. Kuehn, *Nat. Cell Biol.*, 2010, **12**, 1115–22.

3. K. Yamamoto, T. Takahashi, T. Asahara, N. Ohura, T. Sokabe, A. Kamiya, and J. Ando, *J. Appl. Physiol.*, 2003, **95**, 2081–8.

4. F. le Noble, D. Moyon, L. Pardanaud, L. Yuan, V. Djonov, R. Matthijsen, C. Bréant, V. Fleury, and A. Eichmann, *Development*, 2004, **131**, 361–75.

5. J. G. Goetz, E. Steed, R. R. Ferreira, S. Roth, C. Ramspacher, F. Boselli, G. Charvin, M. Liebling, C. Wyart, Y. Schwab, and J. Vermot, *Cell Rep.*, 2014, **6**, 799–808.

6. F. Moazzam, F. a DeLano, B. W. Zweifach, and G. W. Schmid-Schönbein, *Proc. Natl. Acad. Sci. U. S. A.*, 1997, **94**, 5338–43.

7. L. Adamo, O. Naveiras, P. L. Wenzel, S. McKinney-Freeman, P. J. Mack, J. Gracia-Sancho, A. Suchy-Dicey, M. Yoshimoto, M. W. Lensch, M. C. Yoder, G. García-Cardeña, and G. Q. Daley, *Nature*, 2009, **459**, 1131–5.

8. A. Mammoto, T. Mammoto, and D. E. Ingber, *J. Cell Sci.*, 2012.

9. J.-W. Shin, J. Swift, I. Ivanovska, K. R. Spinler, A. Buxboim, and D. E. Discher, *Differentiation*, 2013, **86**, 77–86.

10. A. Gratwohl, H. Baldomero, and J. Passweg, *Curr. Opin. Hematol.*, 2013, **20**, 485–93.

11. A. Trounson, R. G. Thakar, G. Lomax, and D. Gibbons, *BMC Med.*, 2011, **9**, 52.

12. E. a Copelan, *N. Engl. J. Med.*, 2006, **354**, 1813–26.

13. W. J. Polacheck, R. Li, S. G. M. Uzel, and R. D. Kamm, *Lab Chip*, 2013, **13**, 2252–67.

14. W. Liu, L. Li, X. Wang, L. Ren, X. Wang, J. Wang, Q. Tu, X. Huang, and J. Wang, *Lab Chip*, 2010, **10**, 1717–24.

15. V. Lecault, M. Vaninsberghe, S. Sekulovic, D. J. H. F. Knapp, S. Wohrer, W. Bowden, F. Viel, T. McLaughlin, A. Jarandehei, M. Miller, D. Falconnet, A. K. White, D. G. Kent, M. R. Copley, F. Taghipour, C. J. Eaves, R. K. Humphries, J. M. Piret, and C. L. Hansen, *Nat. Methods*, 2011, **8**, 581–6.

16. J. J. VanDersarl, A. M. Xu, and N. a Melosh, *Lab Chip*, 2011, **11**, 3057–63.

17. T. M. Keenan, C. W. Frevert, A. Wu, V. Wong, and A. Folch, *Lab Chip*, 2010, **10**, 116–22.

18. Y.-C. Toh, C. Zhang, J. Zhang, Y. M. Khong, S. Chang, V. D. Samper, D. van Noort, D. W. Hutmacher, and H. Yu, *Lab Chip*, 2007, **7**, 302–9.

19. C. Zhang, Z. Zhao, N. A. Abdul Rahim, D. van Noort, and H. Yu, *Lab Chip*, 2009, **9**, 3185–92.

20. L. Wang, X.-F. Ni, C.-X. Luo, Z.-L. Zhang, D.-W. Pang, and Y. Chen, *Biomed. Microdevices*, 2009, **11**, 679–84.

21. C. Luo, L. Jiang, S. Liang, Q. Ouyang, H. Ji, and Y. Chen, *Biomed. Microdevices*, 2009, **11**, 981–6.

22. M. Kolnik, L. S. Tsimring, and J. Hasty, *Lab Chip*, 2012, **12**, 4732–7.

23. L. Lu, M. Xiao, R. N. Shen, S. Grigsby, and H. E. Broxmeyer, *Blood*, 1993, **81**, 41–8.

24. L. W. Terstappen, S. Huang, M. Safford, P. M. Lansdorp, and M. R. Loken, *Blood*, 1991, **77**, 1218–27.

25. R. G. Andrews, B. Torok-Storb, and I. D. Bernstein, *Blood*, 1983, **62**, 124–32.

26. J. S. Nielsen and K. M. Mcnagny, *J. Cell Sci.*, 2008, **4145**, 3683–3692.

27. A.-V. Fonseca, D. Freund, M. Bornhäuser, and D. Corbeil, *J. Biol. Chem.*, 2010, **285**, 31661–71.

28. F. Sánchez-madrid and J. M. Serrador, *Nat. Rev. Mol. Cell Biol.*, 2009, **10**, 353–359.

29. A.-V. Fonseca and D. Corbeil, *Commun. Integr. Biol.*, 2011, **4**, 201–4.

30. N. Vannini, A. Roch, O. Naveiras, A. Griffa, S. Kobel, and M. P. Lutolf, *Cell Cycle*, 2012, **11**, 1535–43.

31. J. Shin, A. Buxboim, K. R. Spinler, J. Swift, D. A. Christian, C. A. Hunter, C. Léon, C. Gachet, P. C. D. P. Dingal, I. L. Ivanovska, F. Rehfeldt, J. A. Chasis, and D. E. Discher, *Cell Stem Cell*, 2014, **14**, 81–93.

Figure Legends

Figure 1 – No-flow chamber design

(A) Design principle showing the central chamber and the side channels allowing medium supply.
(B) Illustration of the pressure balance condition required for protecting the central chamber from the flow in the side channels (shown as white arrows).
(C) Illustration of medium renewal based on solutes diffusion through chamber openings.
(D) Array of no-flow chambers supplied with symmetric side channels.
(E) Illustration of no-flow chamber filling from symmetric side channels. The liquid is shown in green, the air is in white. Air is trapped in the chamber.
(F) Array of no-flow chambers supplied with asymmetric side channels.
(G) Illustration of no-flow chamber filling from asymmetric side channels. The liquid is shown in green, the air is in white. The delay between the liquid progressions in the two channels prevents air trapping in the chamber.
(H) Video recording of chambers filling by water containing Alexa-488 fluorophores as a marker (shown in green). Blue lines highlight the channel shapes. Time is in second.
(I) Picture of the PDMS chip.
(J) Zoomed picture of the PDMS chip.

Figure 2 – Flow measurement in the no-flow chambers

(A) One-micron polystyrene beads were used as fiduciary markers to reveal fluid flow. Images were taken with 200 ms exposure time (see movie S2) to record bead trajectories. The displayed image is the overlay of 10 images taken with 500 ms time interval in order to reveal the field lines. They do not enter the no-flow chambers.
(B) Bead motion movies were recorded at various positions in the chip, at the entry (left), in the middle (center) and at the exit (right) of the micro-channels and used to record bead velocities in the chambers.
(C) Bead velocities were measured in all chambers along the micro-channels for two inlet fluid velocities: 150 µm/s (left) and 1500 µm/s (right). Data showed that flow was null in the 30 central chambers.

Figure 3 – Medium renewal

(A) The chip was filled with 1 µM of Alexa-488 (green fluorescence emission) in water. The inlet was then switch to 1 µM Alexa-568 (red fluorescence emission) in water. Green and red fluorescence in the chambers was video-recorded. Time is indicated in min:sec.
(B) Green and red fluorescence emissions were measured in the no-flow chamber (position A) and in the side channel (position B). Intensity values were normalized to the initial or final values for green and red respectively. Dashed lines show the fluorescence in the side channel. Full lines show the fluorescence in the no-flow chambers. It took about 7 minutes after inlet switch to renew completely the medium in the chambers.

Figure 4 – HSC growth in no-flow chambers

(A) Observation of HSCs (arrows) in transmitted light after no-flow chamber filling.
(B) Video recording of HSC in a no-flow chamber in transmitted light. Time is in hours. Scale bar is 50 µm.
(C) Live HSC staining with fluorescent primary antibodies against CD38 (green), CD34 (blue) and CD33 (red) at the end of the video recording. Antibodies were added to the culture medium in the side channels. Scale bar is 50 µm.

(D) Quantification of the proportion of cells expressing the various makers after 3 days of culture in no-flow chambers. Color code is shown at the bottom. N = 257 cells, n = 17 chambers.
(E) Example of a lineage tree obtained after visual tracking of HSCs in the no-flow chambers. Bottom line shows cells staining at the end of the movie. Color code is shown at the bottom.
(F) Quantification of the surface receptor expression profiles depending on the number of cell division during the three days of observation. N = 257 cells, n = 17 chambers.

Figure 5 – HSC polarization

(A) Quantification of the surface receptor expression profiles in static and migrating cells. N = 257 cells, n = 17 chambers.
(B) Images showing the spatial distribution of CD34 (blue) and CD33 (red) at the surface of stating and migrating HSCs after three days of culture in no flow-chambers.
(C) Measurement of cell aspect ratio (top line) and localization of surface markers (bottom line) in static and migrating HSCs. Cell aspect ratio was measured by fitting cell shape with an ellipse and quantifying the ratio of the short and long axes. Migrating cells appeared more elongated. Surface marker localization was quantified by measuring the coordinate of the center of mass of the fluorescence signal along the long cell axis (x_{cm}) and normalizing it to the length of this axis. CD33 appeared systematically polarized in the rear of migrating HSCs.

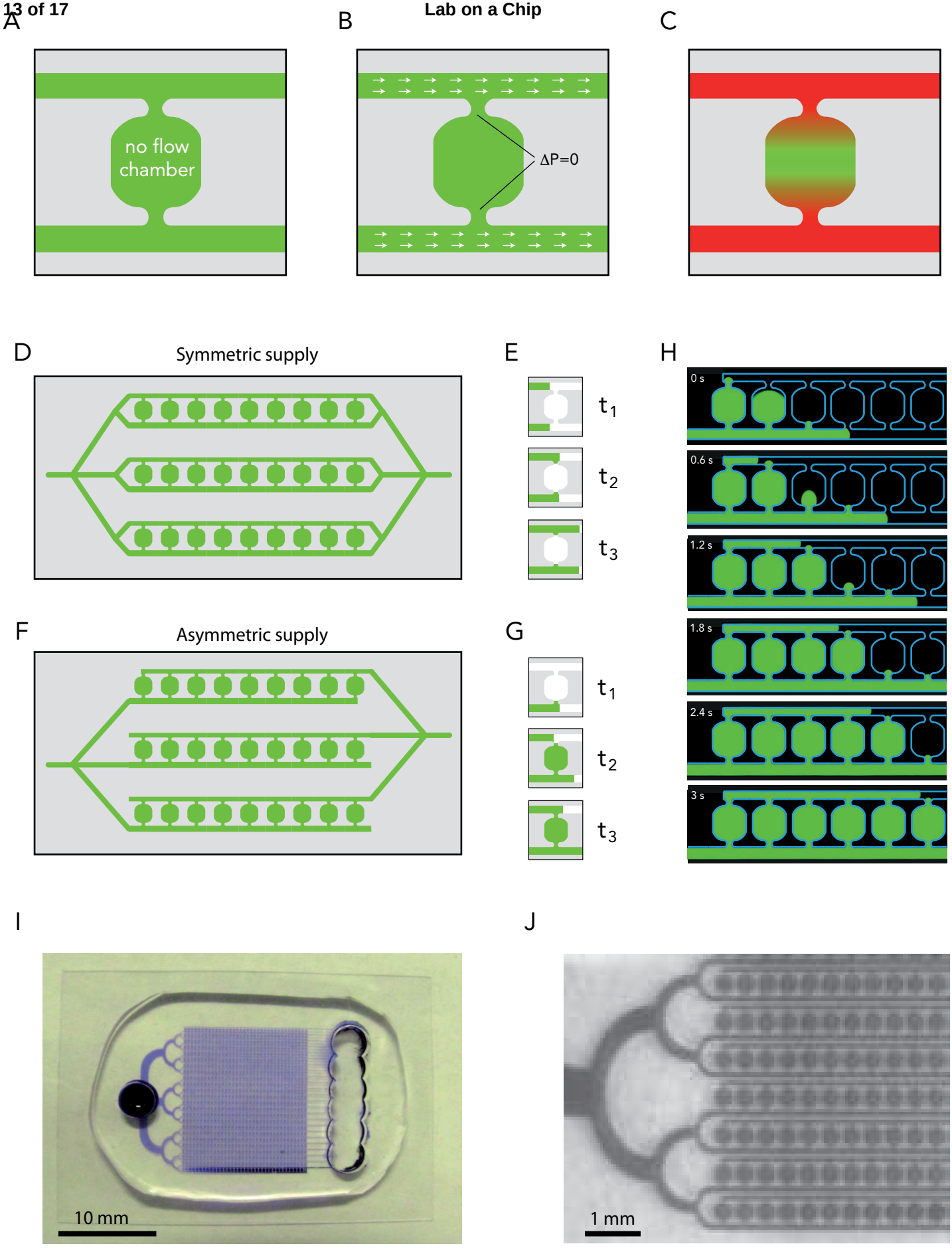
A
no flow chamber
B
ΔP=0
C
D
Symmetric supply
E
t1
t2
t3
H
0 s
0.6 s
1.2 s
1.8 s
2.4 s
3 s
F
Asymmetric supply
G
t1
t2
t3
I
10 mm
J
1 mm

A

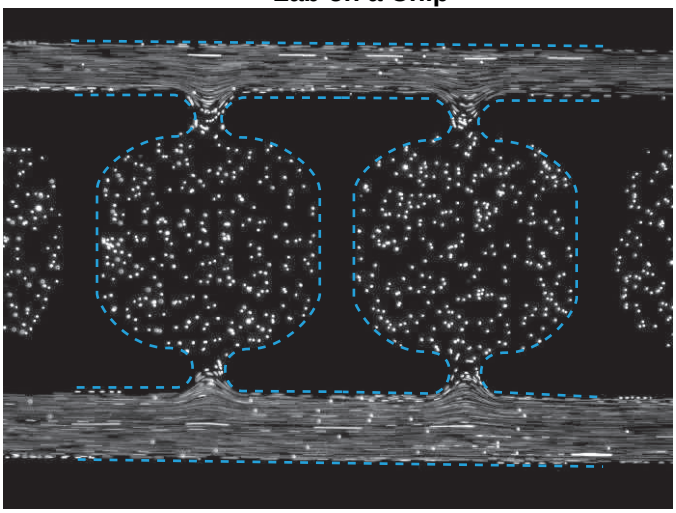

B

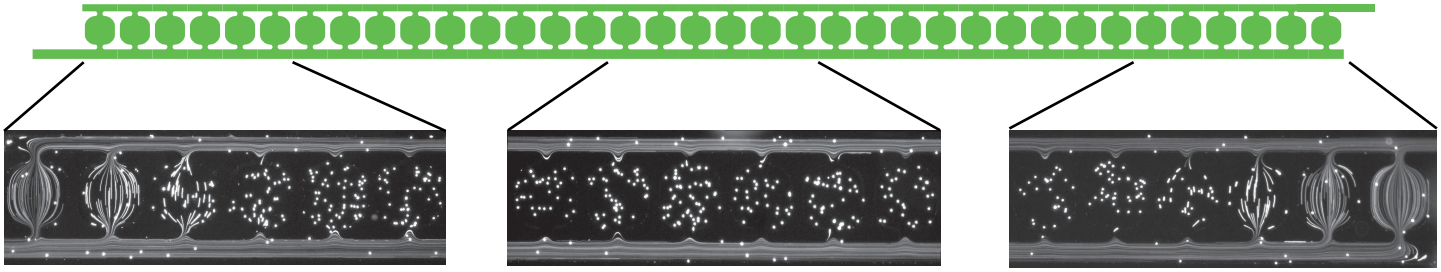

C

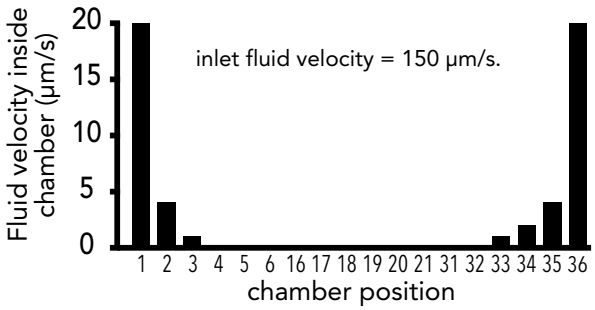
Fluid velocity inside chamber (μm/s)
20
15
10
5
0
inlet fluid velocity = 150 μm/s.
1 2 3 4 5 6 16 17 18 19 20 21 31 32 33 34 35 36
chamber position

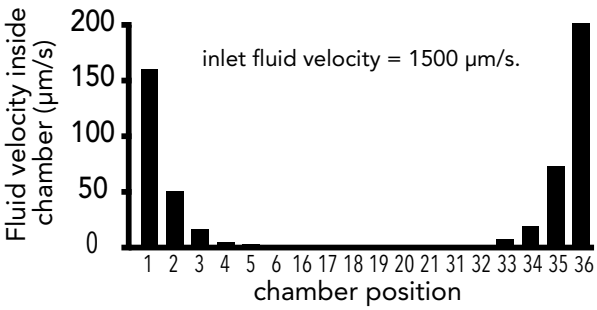
Fluid velocity inside chamber (μm/s)
200
150
100
50
0
inlet fluid velocity = 1500 μm/s.
1 2 3 4 5 6 16 17 18 19 20 21 31 32 33 34 35 36
chamber position

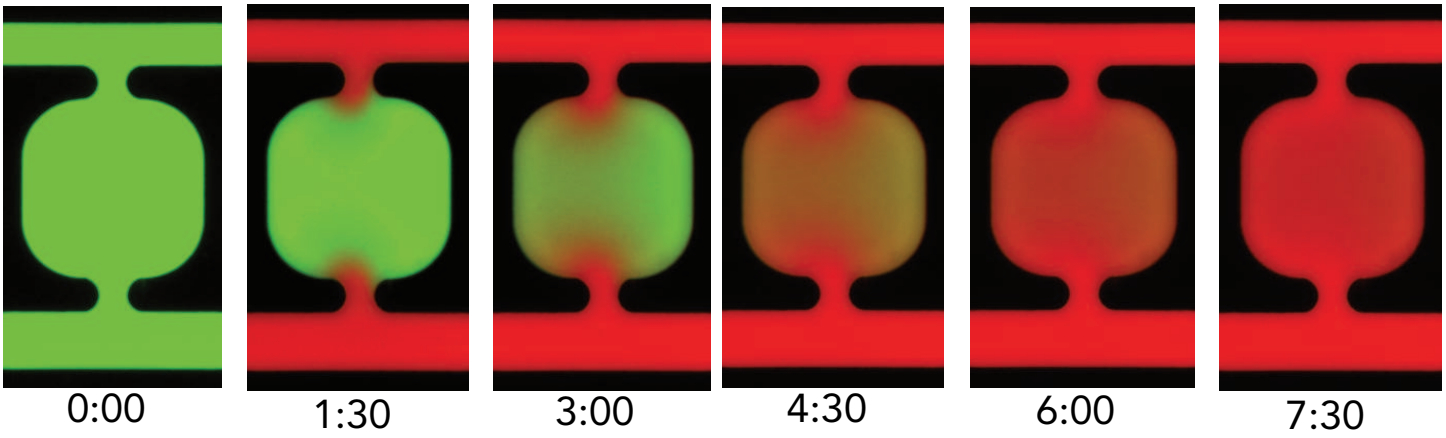
0:00
1:30
3:00
4:30
6:00
7:30

B

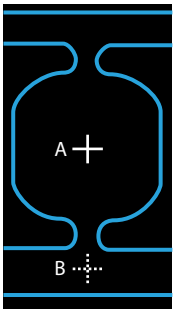
A
B

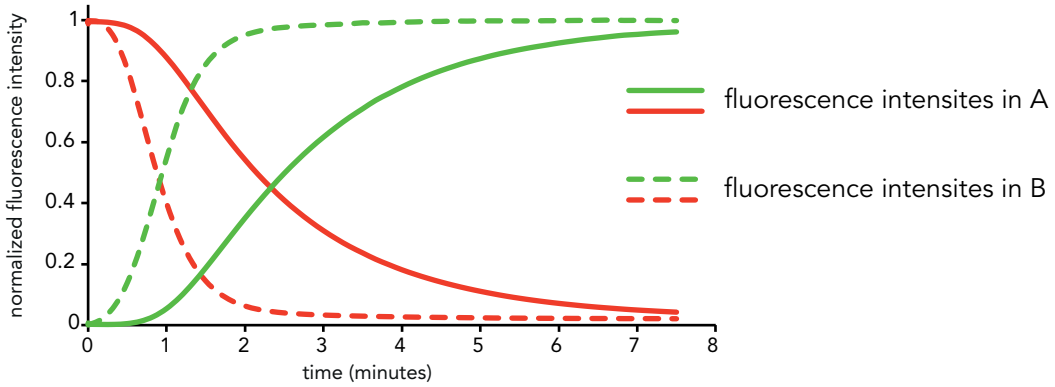
normalized fluorescence intensity
1
0.8
0.6
0.4
0.2
0
0
1
2
3
4
5
6
7
8
time (minutes)
fluorescence intensites in A
fluorescence intensites in B

A

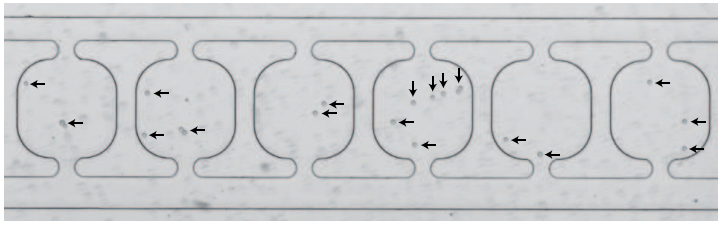

B

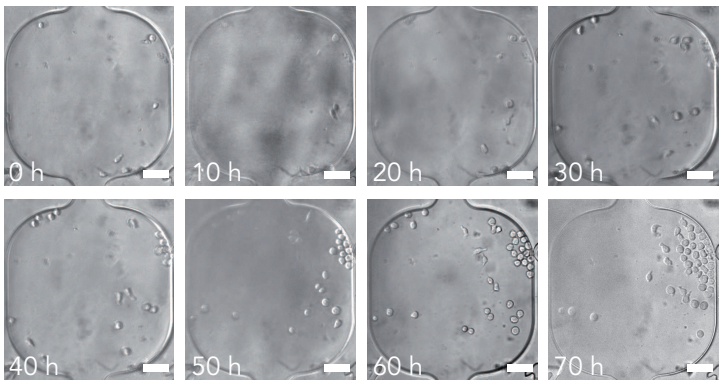
0 h
10 h
20 h
30 h
40 h
50 h
60 h
70 h

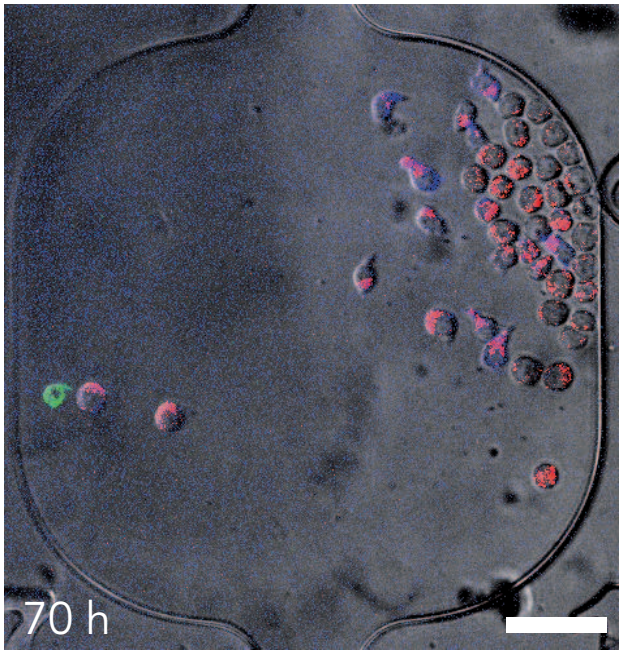
70 h

D

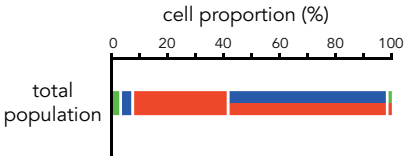
cell proportion (%)
0
20
40
60
80
100
total population

F

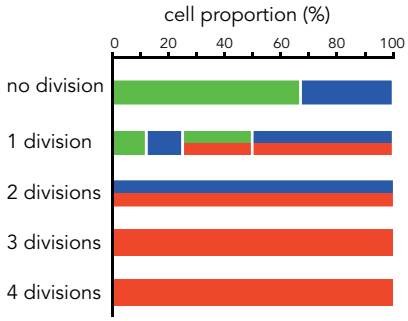
cell proportion (%)
0
20
40
60
80
100
no division
1 division
2 divisions
3 divisions
4 divisions

E

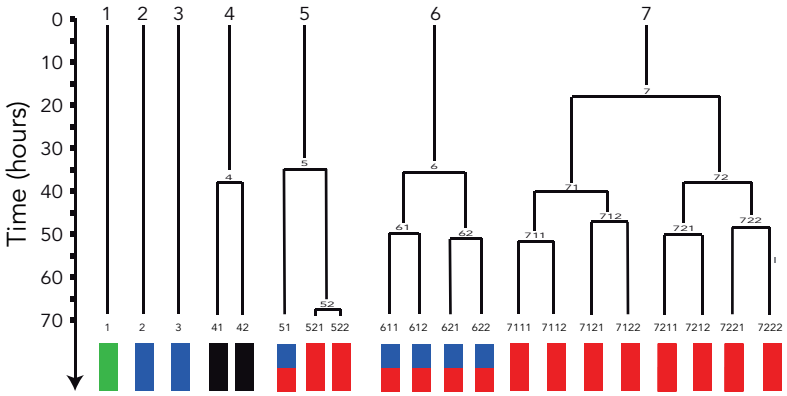
Time (hours)
0
10
20
30
40
50
60
70
1
2
3
4
5
6
7
1
2
3
41
42
51
521
522
611
612
621
622
7111
7112
7121
7122
7211
7212
7221
7222


CD38+
CD34+
CD33+
CD33+/CD34+
CD33+/CD38+
no signal

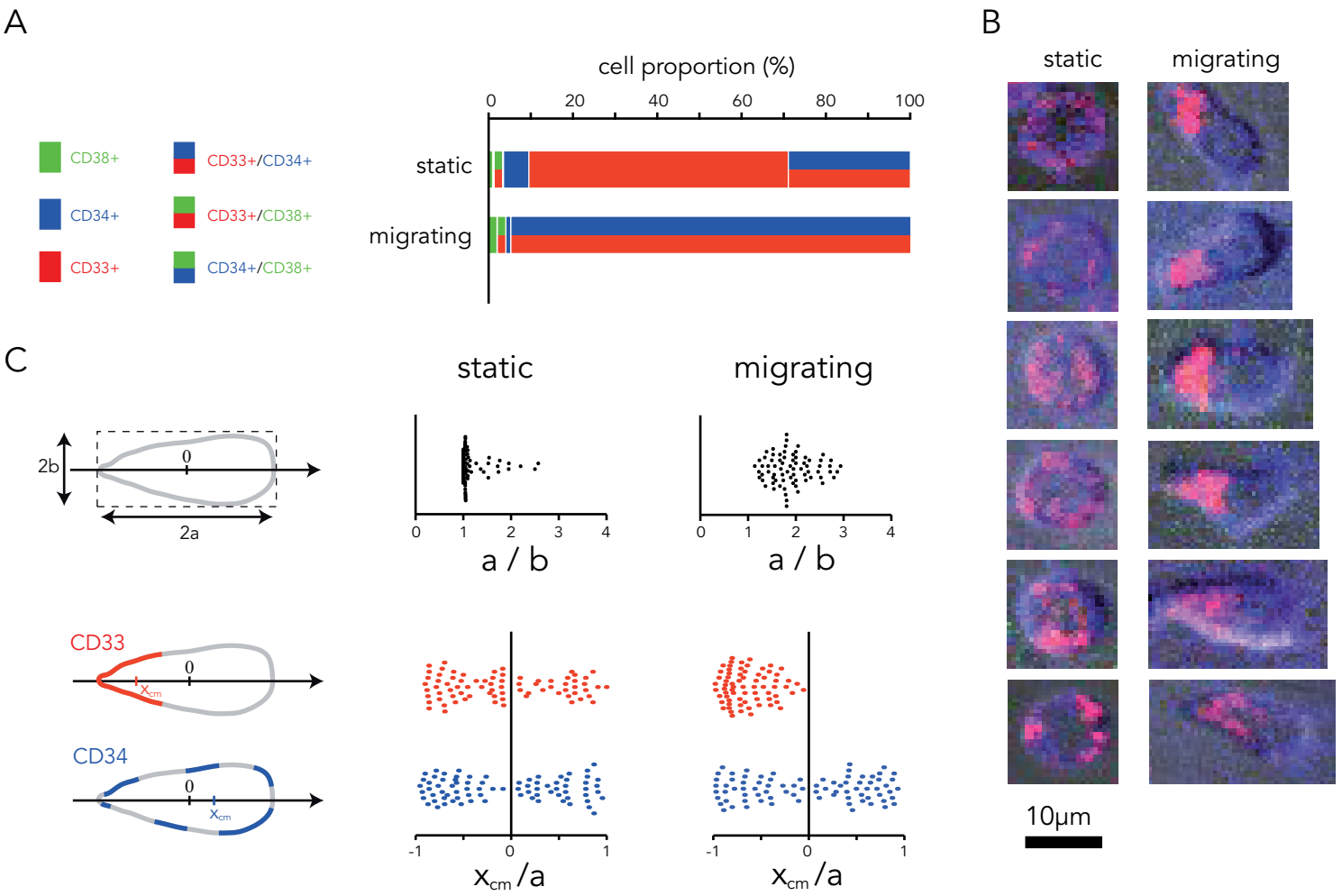
A
CD38+
CD33+/CD34+
CD34+
CD33+/CD38+
CD33+
CD34+/CD38+
cell proportion (%)
0 20 40 60 80 100
static
migrating
B
static
migrating
10μm
C
static
migrating
2b
2a
0
CD33
CD34
a / b
a / b
x_{cm} /a
x_{cm} /a